To the Referee

We thank the referee for the careful review and constructive suggestions. Below, we respond to each point in detail and indicate the corresponding changes in the manuscript.

Comment: *This manuscript proposes a theoretical model for realizing 2D higher-order Weyl semimetals (HOWSMs) via a trilayer topological film (inspired by Bi2Se3) coupled to a d-wave altermagnet. The pristine film exhibits 2D Weyl semimetals with helical edge states and four Weyl points. Introducing z-directed d-wave altermagnetism gaps the edges, preserves two Weyl points, and induces corner states, characterized by subspace winding numbers. A phase diagram delineates HOWSM and standard Weyl semimetal phases. The work is novel in extending higher-order topology to 2D gapless systems, leveraging altermagnets, a recently proposed magnetic order, for momentum-selective edge gapping while preserving bulk Weyl nodes. This "gapless-bulk, gapped-boundary" paradigm is intriguing and could inspire hybrid topological-magnetism studies. The subspace decomposition via algebraic symmetry M enables analytical invariants (Chern/winding numbers), providing clear topological classification. Numerical results (band structures, nanoflakes) consistently support claims.*

Response: We thank the referee for the clear summary and for recognizing the novelty and conceptual interest of our work.

Comment 1: *A key weakness is the phenomenological nature: the Hamiltonian, while symmetry-guided, lacks tight-binding derivation from realistic materials, limiting experimental relevance (e.g., Bi2Se3 trilayers may not match exactly).*

Response: Thank you for highlighting this important point. We fully agree that deriving a concrete tight-binding model (or ab initio parametrization) from a real material is essential for eventual experimental realization. However, we respectfully submit that a full materials-specific derivation is beyond the intended scope of the present manuscript. The primary aim of our work is to demonstrate a new conceptual mechanism, namely, how a d-wave altermagnetism coupled to a topological-insulator film can generate a two-dimensional higher-order Weyl/topological phase with corner states. To support this idealized mechanism, we adopt a symmetry-guided low-energy Hamiltonian, which allows us to map out the phase diagram clearly and unambiguously.

To partially address the reviewer's concern, we have added a brief discussion that magnetic topological insulator heterostructures may offer a plausible route to access the key building blocks assumed in our model, such as TI films such as Bi_2Se_3 or related compounds and the possibility of interfacing them with candidate altermagnets. In particular, first principles studies of MnTe/Bi_2(Se,Te)$_3$/MnTe heterostructures have demonstrated substantial proximity exchange effects and closely related topological phases, providing realistic guidance on achievable exchange gaps and symmetry breaking energy scales in MnTe and Bi_2Se_3 family interfaces [80]. Experimental ARPES on antiferromagnet and topological insulator heterostructures has also reported a sizable gap opening at the Dirac point in MnSe/Bi_2Se_3, supporting the feasibility of interface engineered exchange gaps [81]. These results do not yet constitute a material specific realization of our higher order Weyl semimetal phase with coexisting bulk Weyl points and corner states, but they provide concrete motivation that the essential ingredients required by our mechanism are experimentally accessible.

We appreciate the referee's suggestion and add a concise statement in the Conclusions, together with the above materials motivation, clarifying that identifying concrete material realizations through systematic ab initio calculations is left for future work (see page 9, column 2, paragraph 1, last lines 1-15). Additionally, we have added the following references:

[80] N. Pournaghavi, M. F. Islam, R. Islam, C. Autieri, T. Dietl, and C. M. Canali, Realization of the Chern-insulator and axion-insulator phases in antiferromagnetic MnTe/Bi_2(Se,Te)$_3$/MnTe heterostructures, Phys. Rev. B **103**, 195308 (2021).

[81] A. V. Matetskiy, I. A. Kibirev, T. Hirahara, S. Hasegawa, A. V. Zotov, and A. A. Saranin, Direct observation of a gap opening in topological interface states of MnSe/Bi_2Se_3 heterostructure, Appl. Phys. Lett. **107**, 091604 (2015).

Comment 2: *The M symmetry is artificial (not crystal-derived), potentially over-idealized; its realizability in van der Waals structures needs justification.*

Response: We appreciate the referee's insightful comment on this issue. As correctly noted, M is not a crystallographic mirror symmetry but an algebraic internal symmetry acting in the layer–spin subspace of the effective Hamiltonian. It arises from the fact that H(k) and M commute, which allows the model to be block-diagonalized into symmetry-respecting subspaces. Such algebraic symmetries are commonly employed in multilayer topological models and engineered platforms where internal degrees of freedom can be precisely controlled.

To clarify its physical realizability, we have added a statement in the revised manuscript explaining that symmetric trilayer van der Waals heterostructures naturally

provide the structural conditions for realizing the algebraic structure encoded by M. In such systems, the two outer layers can be made symmetry-related by stacking design, while the interlayer hybridization can be tuned via stacking geometry, spacer layers, or electrostatic gating, leading to an effective Hamiltonian with the same block structure generated by M (see page 3, column 2, last paragraph, last lines 1-6 and page 4, column 1, lines 1-4).

Comment 3: *Logic is mostly consistent, but inconsistencies arise: Weyl points are claimed at high-symmetry points, yet 2D Weyl nodes typically require accidental crossings—verify if dispersions are truly linear (Fig. 2(a) suggests quadratic touches at some points).*

Response: We appreciate the referee's careful observation regarding the nature of the gapless nodes. To clarify the nature of the gapless nodes, we have performed an explicit low-energy expansion of the subspace Hamiltonian

$$H_0 = -v_F \sin k_y \, \tau_x + v_F \sin k_x \, \tau_y$$

around the four high-symmetry points Γ, X_1, X_2, and M. Writing $\boldsymbol{k} = \boldsymbol{k_W} + \boldsymbol{q}$, we obtain

$$H_0^W(q) \simeq v_F\left(\alpha_W q_x \tau_y + \beta_W q_y \tau_x\right), \qquad |q| \ll 1,$$

where $(\alpha_W,\ \beta_W)$ = (+1,-1), (-1,-1), (+1,+1), and (-1,+1) for W= Γ, X_1, X_2, and M, respectively. The corresponding spectrum

$$E_{\pm}^W(\boldsymbol{q}) = \pm v_F \sqrt{q_x^2 + q_y^2}$$

is strictly linear in q, confirming that all four degeneracies are genuine two-dimensional Weyl crossings rather than quadratic band-touching points.

We have added a paragraph in the revised manuscript presenting this low-energy expansion and explicitly stating that the Weyl points are linear crossings pinned to the high-symmetry momenta (see page 4, column 1, paragraph 1, last lines 4-14).

Comment 4: *Altermagnet justification is perturbative but assumes uniform J; real proximity effects may vary. Phase diagram boundaries (|m0|=4/8|m1|) derive from subspace closures, but exclude J dependence—small J is stated not to affect it, yet Fig. 3 uses J=0.6, risking oversight for larger J.*

Response: We thank the referee for these important remarks. In our model, the d-wave

altermagnetic term enters the $H_{\pm 1}$ subspaces only through a τ_z mass proportional to the form factor $\Delta(k) = \cos k_x - \cos k_y$, while the bulk gap closings of H_0 and $H_{\pm 1}$ are governed solely by the mass $\mathrm{m}(k) = m_0 + 4m_1 - 2m_1(\cos k_x + \cos k_y)$. At the momenta where the subspace gaps close and the Weyl points appear, $\Delta(k)$ vanishes identically, so the altermagnetic exchange field does not modify the gap-closing conditions. As a result, the phase boundaries $|m_0| = 4|m_1|$ and $|m_0| = 8|m_1|$ are strictly independent of J as long as no additional accidental gap closings are induced away from these high-symmetry lines.

To substantiate this point, we have explicitly checked that no extra bulk gap closings occur throughout the Brillouin zone for $|J| \leq 1$ (see Fig. R1), which comfortably covers the range of realistic proximity-induced exchange energies. The value J=0.6 used in Figs. 3 and 4 therefore lies safely within the regime where the phase diagram in Fig. 5(d) remains unchanged. We have revised the discussion around Fig. 5(d) to explain this mechanism and to clarify the J-independence of the phase boundaries in the physically relevant parameter range (see page 8, column 2, paragraph 2, last lines 1-7).

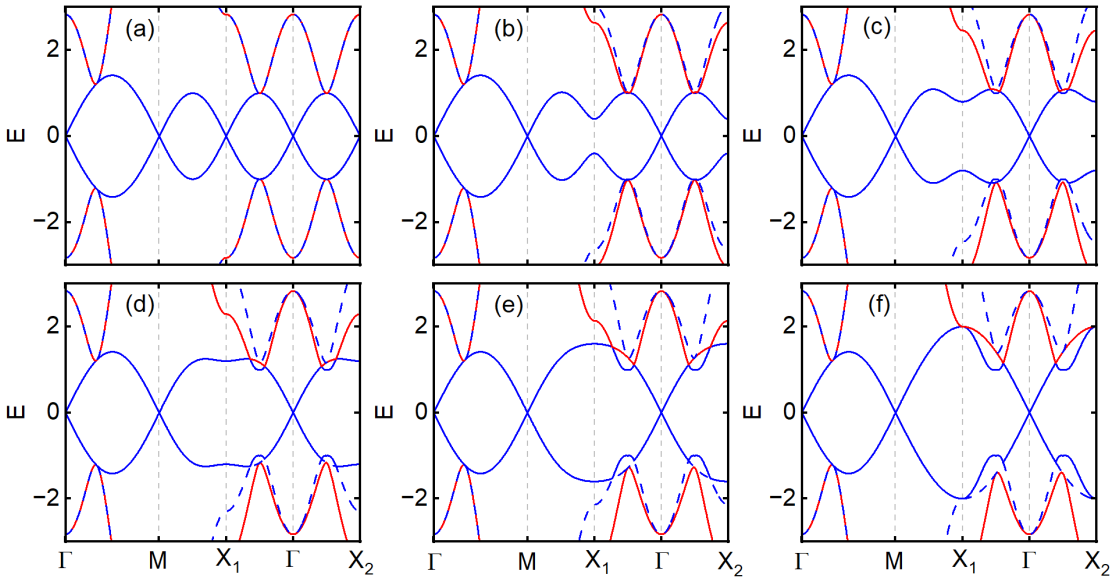

Figure R1. *Bulk band structures of the trilayer model for different strengths of the altermagnetic exchange field J. Panels (a)–(f) correspond to J=0, 0.2, 0.4, 0.6, 0.8, and 1.0, respectively. The two Weyl points at Γ and M remain gapless for all J≤1, while the Weyl points at X_1 and X_2 gap out once J≠0. No additional gap closings emerge elsewhere in the Brillouin zone as J increases, demonstrating that the phase boundaries are independent of J over the physically relevant range.*

Comment 5: *No discussion of disorder/interaction effects on corner states.*

Response: We appreciate the referee's thoughtful comment on this point. In the revised manuscript we have added a new subsection "Robustness against disorder" (see page 7, Sec. III D) and a new Fig. 4. For clarity, the version of this figure included in the present reply is labeled figure. R2. There we clarify that the corner states originate from a quantized winding number defined in the M-symmetric subspaces of the effective Hamiltonian and are therefore stable against symmetry-preserving perturbations. A random magnetic disorder $H_{dis} = \sum_i w_i c_i^\dagger c_i$, $w_i \in [-W, W]$,which respects the M-subspace structure, leaves the four in-gap levels pinned near zero energy and sharply localized at the corners over a wide range of disorder strength, as shown in Fig. R2 (a,b).

In contrast, scalar onsite-potential disorder acts identically on all internal degrees of freedom, mixes different M subspaces, and couples the corner modes to the gapless bulk continuum. For sufficiently strong W the four in-gap levels broaden and merge into the bulk spectrum, indicating that the corner states are not stable against generic, symmetry-breaking scalar disorder in a gapless system. This behavior reflects a generic feature of gapless higher-order Weyl semimetals rather than a particular fine-tuning of our model. A systematic analysis of interaction-driven phases is beyond the scope of the present work and is left for future study.

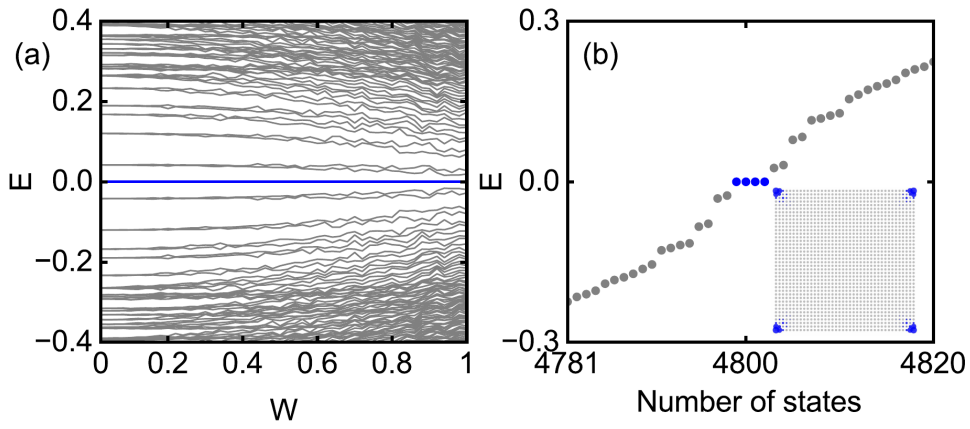

Figure R2. *(a) Energy spectrum of a 40a × 40a nanoflake as a function of the strength W of the random magnetic disorder. Gray lines denote bulk and edge states, while the four corner levels are highlighted in blue. The corner states remain pinned near zero energy over a wide range of W. (b) Eigenvalue spectrum near zero energy for a fixed disorder strength W = 0.5. Blue dots mark the four corner states, and the inset shows their wave-function probability distribution, localized at the four corners of the nanoflake.*

Advice for Improvement:

Comment 1: *Link model to specific materials (e.g., MnTe/Bi2Se3 interfaces) with ab initio estimates for parameters.*

Response: We appreciate this helpful suggestion. As clarified in our response to the previous comment, we have added a brief discussion in the revised manuscript pointing out that magnetic topological insulator heterostructures, such as $MnTe/Bi_2(Se,Te)_3/MnTe$ stacks, provide a plausible materials platform where the key ingredients of our symmetry guided minimal model naturally arise. We also cite first principles and experimental works illustrating proximity induced exchange gaps in such interfaces. At the same time, obtaining quantitative ab initio parameter estimates for a specific heterostructure requires a dedicated materials study, which is beyond the scope of our mechanism focused work. To make this point explicit, a brief clarification has been added in the revised manuscript (see page 9, column 2, paragraph 1, last lines 1-15).

Comment 2: *Analytically derive corner state wavefunctions or use effective models for edges.*

Response: In the revised manuscript, we have added an explicit edge-theory analysis to make the presentation more complete. Starting from the trilayer lattice Hamiltonian, we derive its low-energy continuum form, project onto the helical-edge subspace, and obtain effective 1D Dirac Hamiltonians on the four edges with altermagnet-induced mass terms. The resulting masses alternate in sign between adjacent edges, so each corner hosts a Jackiw–Rebbi mass domain wall and therefore supports a localized zero-energy bound state. This analytic edge theory provides the requested effective model and accounts for the corner modes observed in our numerical calculations.

The full derivation has been included in the new subsection “Edge theory” in Sec. III (see page 6-7), and Ref. [77] has been added to cite the Jackiw-Rebbi mechanism.

[77] R. Jackiw and C. Rebbi, Solitons with fermion number 1/2, Phys. Rev. D 13, 3398 (1976).

Comment 3: *Expand experimental probes: beyond STM, suggest transport (e.g.,*

nonlocal resistance for corners) or ARPES for Weyl nodes.

Response: We appreciate this helpful suggestion. In addition to the STM signatures already mentioned, we have expanded the discussion of experimentally accessible probes. The localized corner modes are expected to produce resonant transport features, including sharp conductance peaks under gate tuning and enhanced nonlocal resistance between corner contacts in multiterminal geometries. This expanded discussion has been added to the revised manuscript (see page 9, column 1, paragraph 1, lines 10-15).

Comment 4: *Address finite-size effects on hybridization.*

Response: We agree that finite-size effects can induce a small splitting of the nominally zero-energy corner modes through weak hybridization. To evaluate this, we computed the lowest-energy positive eigenvalue (i.e. the corner state energy splitting) for several nanoflake sizes $n = N_x = N_y$ within the range used in our study. The resulting size dependence (see Fig. R3) shows a rapid suppression of the splitting with increasing n, indicating that the system sizes employed in the manuscript already place the corner-state energies well below numerical resolution. This behavior confirms that finite-size effects do not affect our conclusions. A brief clarification has been added to the revised manuscript (see page 5, column 1, paragraph 2, last lines 3-8).

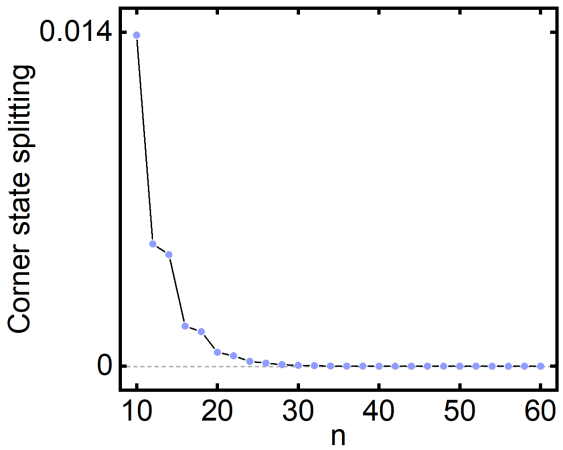

Figure R3. *Size dependence of the corner-state energy splitting for a square nanoflake with linear size* $n = N_x = N_y$. *The splitting decreases rapidly with increasing* n *and becomes negligibly small for the system sizes used in the manuscript* ($n \geq 30$), *indicating that the corner modes are effectively degenerate and well isolated in our calculations.*

Comment 5: *Revise for clarity: define "higher-order" explicitly in 2D context;*

Response: We appreciate this helpful suggestion. In the revised manuscript, we have clarified the definition of higher-order topology and its specific meaning in two dimensions. In the Introduction, we now explicitly state that a d-dimensional *n*th-order topological phase is characterized by gapless boundary modes living on (d-n)-dimensional boundaries, rather than on the conventional (d-1)-dimensional ones. We further specify that, in two dimensions, a second-order topological phase has all one-dimensional edges gapped while zero-dimensional corner states appear inside the edge excitation gap. This revision makes the notion of "higher-order" in the 2D context precise and directly linked to the corner states discussed in this work (see page 1, column 1, paragraph 1, lines 7-13).

Comment 6: *add error bars or convergence checks for numerics.*

Response: We appreciate this helpful suggestion. All numerical results in our work are obtained from deterministic tight-binding calculations (exact diagonalization and Brillouin-zone integration), rather than from stochastic sampling, so conventional statistical error bars are not applicable. The main quantities we compute, including the band structures, edge and corner spectra, and the integer-valued topological invariants (Chern numbers and winding numbers), remain stable under numerical refinement.

In particular, the Chern and winding numbers do not change when the Brillouin-zone mesh is made denser, and the number and spatial localization of the corner states are insensitive to the nanoflake size used in our calculations. These points are now stated explicitly in the revised manuscript (see page 4, column 2, paragraph 2, last lines 3–6; page 5, column 1, paragraph 1, last lines 1–4).

In addition, Sec. III D of the revised manuscript includes an explicit analysis of disorder effects (see page 7, column 1-2). Figure 4 shows that random magnetic disorder keeps the four corner levels pinned near zero energy and sharply localized at the corners across a wide range of disorder strengths, confirming the robustness of the higher-order boundary modes against symmetry-preserving perturbations.